Anisotropic fluxes and nonlocal interactions in magnetohydrodynamic turbulence

A. Alexakis,[1] B. Bigot,[1,2] H. Politano,[1] and S. Galtier[2]

[1]*Laboratoire Cassiopée, UMR 6202, Observatoire de la Côte d'Azur, Boîte Postale 4229, Nice Cedex 4, France*
[2]*Institut d'Astrophysique Spatiale (IAS), Université Paris-Sud XI and CNRS (UMR 8617), Bâtiment 121, F-91405 Orsay, France*

We investigate the locality or nonlocality of the energy transfer and the spectral interactions involved in the cascade for decaying magnetohydrodynamic (MHD) flows in the presence of a uniform magnetic field **B** at various intensities. The results are based on a detailed analysis of three-dimensional numerical flows at moderate Reynolds numbers. The energy transfer functions, as well as the global and partial fluxes, are examined by means of different geometrical wave number shells. On the one hand, the transfer functions of the two conserved Elsässer energies E^+ and E^- are found local in both the directions parallel ($k_\parallel$ direction) and perpendicular ($k_\perp$ direction) to the magnetic guide field, whatever the **B** strength. On the other hand, from the flux analysis, the interactions between the two counterpropagating Elsässer waves become nonlocal. Indeed, as the **B** intensity is increased, local interactions are strongly decreased and the interactions with small $k_\parallel$ modes dominate the cascade. Most of the energy flux in the $k_\perp$ direction is due to modes in the plane at $k_\parallel=0$, while the weaker cascade in the $k_\parallel$ direction is due to the modes with $k_\parallel=1$. The stronger magnetized flows tend thus to get closer to the weak turbulence limit, where three-wave resonant interactions are dominant. Hence, the transition from the strong to the weak turbulence regime occurs by reducing the number of effective modes in the energy cascade.

I. INTRODUCTION

The existence of magnetic fields is known in many astrophysical objects, such as the interstellar medium, galaxies, accretion disks, star and planet interiors, or solar wind (see, e.g., [1]). In most of these systems, the magnetic fields are strong enough to play a significant dynamical role. The kinetic and magnetic Reynolds numbers involved in these astrophysical bodies are large enough so that the flows exhibit a turbulent behavior with a large continuous range of excited scales, from the largest where energy is injected, toward the finest where energy is dissipated. In many cases, a strong large-scale magnetic field is present and induces dynamic anisotropy. Direct numerical simulations that examine in detail the turbulent processes in geo- and astrophysical plasmas are very difficult to achieve, and only modest Reynolds numbers can be reached with today's computers. One way around this difficulty is to model the small spatial and temporal scales to reproduce the large-scale behavior of turbulent flows. A more basic understanding of turbulence is thus needed to adequately model the flows, in particular when a uniform magnetic field, constant in both space and time, is applied.

As a first approximation, the incompressible magnetohydrodynamic (MHD) equations can be used to describe the evolution of both velocity **u** and magnetic field **b** fluctuations. In the presence of a uniform magnetic field **B** (magnetic fields are here expressed in velocity units), the Elsässer formulation of the MHD equations, with constant unit mass density, reads

$$\partial_t \mathbf{z}^\pm = \pm \mathbf{B} \cdot \nabla \mathbf{z}^\pm - \mathbf{z}^\mp \cdot \nabla \mathbf{z}^\pm - \nabla P + \frac{\nu+\eta}{2}\nabla^2\mathbf{z}^\pm + \frac{\nu-\eta}{2}\nabla^2\mathbf{z}^\mp,$$

(1)

together with $\nabla \cdot \mathbf{z}^\pm = 0$, where $\mathbf{z}^\pm = \mathbf{u} \pm \mathbf{b}$ are the Elsässer fluctuations, which describe Alfvén waves moving along the direction of the magnetic field (z^+) or along the direction opposite to the magnetic field (z^-). P is the total (kinetic plus magnetic) pressure. We assume here equal molecular viscosity ν and magnetic diffusivity η, in other words, a unit magnetic Prandtl number ($P_r = \nu/\eta = 1$). Hereafter, the direction along the **B** magnetic field is referred to as the parallel direction and the projection of the wave vectors along this direction is denoted $k_\parallel$, while the two directions of planes perpendicular to **B** are referred to as perpendicular directions, the wave vector projection onto such planes being denoted $\mathbf{k}_\perp$ with norm $k_\perp \equiv |\mathbf{k}_\perp|$.

For periodic boundary conditions, Eqs. (1) have two independent invariants in the absence of molecular viscosity and magnetic diffusivity, namely, the Elsässer energies

$$E^\pm = \frac{1}{2}\int \mathbf{z}^{\pm 2}(\mathbf{x})dx^3.$$

(2)

It is worth noting here that the two energies are independently conserved and there is no transformation of one energy to the other. In a collision between two oppositely directed waves, the waves will be distorted, resulting in structures of smaller scales, but the energy of each wave will remain the same. Thus, although the interaction of oppositely directed waves is necessary for the cascade of energy to smaller scales, oppositely directed waves themselves do not exchange energy. When very small viscosity and magnetic diffusivity are present, it is expected that the interactions of the Alfvén waves cascade the energies in the so-called inertial range, down to the smallest scales, where dissipation becomes effective and removes energy from the system. The rate at which large scales lose energy is then controlled by the nonlinear terms $\mathbf{z}^\mp \cdot \nabla \mathbf{z}^\pm - \nabla P$ that are responsible for coupling different scales and cascading the energy toward the dissipative scales. The nature of the interactions among

various scales in turbulent flows that lead to this cascade is a long-standing problem. Understanding the mechanisms involved is very important to predict evolution of the large-scale flow behavior, and to estimate global quantities in astrophysical systems, such as the transport of angular momentum, and accretion rates in accretion disks.

High-Reynolds-number hydrodynamic turbulence, often investigated in the framework of statistically homogeneous and isotropic turbulence (which can be a questionable assumption in natural flows), is described to first order by the Kolmogorov theory [2]. In this phenomenological description, interactions between eddies of similar size give the dominant contribution to the energy cascade. This assumption leads to an energy spectrum in $k^{-5/3}$ and an energy cascade rate proportional to u_{rms}^3/L, where u_{rms} is the root mean square of the velocity at large scale and L is the typical (large) flow scale.

The cascade in MHD turbulence is more complex, especially in the presence of a background magnetic field. Even in the simplest case of zero or small intensity of the **B** field, so that isotropy could be recovered, whether the MHD energy cascade can be described by a Kolmogorov type of phenomenology is still an open question. In particular, the assumption that interactions between similar-size eddies (local interactions) are responsible for the cascade of energy to smaller scales has been questioned in turbulent MHD flows by both theoretical arguments [3–5] and the use of numerical simulations [6–8]. It has been shown for mechanically forced MHD turbulence that there is a strong nonlocal coupling between the forced scales and the small scales of the inertial range. Moreover, the large-scale magnetic field generated by the dynamo action can also locally affect the small scales by suppressing the cascade rate in the same manner that an initially imposed uniform magnetic field would. In the other limit, a strong **B** field can lead to flow bidimensionalization, with a drastic reduction of the nonlinear transfers along the uniform magnetic field. For a **B** intensity (denoted B) well above the rms level of kinetic and magnetic fluctuations, the MHD turbulence may be dominated by the Alfvén wave dynamics, leading to wave (or weak) turbulence where the energy transfer, stemming from three-wave resonant interactions, can only increase perpendicular components of the wave vectors, i.e., components in planes perpendicular to the **B** direction ($k_\perp$ direction), the nonlinear transfers along **B** ($k_\parallel$ direction) being completely inhibited [9–11]. How MHD turbulence moves from the weak turbulence limit $B \gg u_{rms}$ to the strong turbulence limit $B \sim u_{rms}$ and $B \sim 0$ (where isotropy could be recovered) is an open question.

Various authors have tried to give a physical description of the strong turbulence regime with $B \sim u_{rms}$. Iroshnikov [12] and Kraichnan [13] first proposed a phenomenological description that takes into account the effect of a large-scale magnetic field by reducing the rate of the cascade due to the short time duration of individual collisions of $z^\pm$ wave packets. The resulting one-dimensional (1D) energy spectrum is then given by $E(k) \sim (\epsilon B)^{1/3} k^{-3/2}$. However, this description assumes isotropy and, while the effect of the large-scale field is taken into account by reducing the effective amplitude of the interactions, the interactions themselves are considered to be local. In order to take into account anisotropy in strong

turbulence, a scale-dependent anisotropy has been proposed [14], the turbulent $z_l^\pm$ eddies being such that the associated Alfvén $\tau_A \sim l_\parallel/B$ and nonlinear $\tau_{NL} \sim l_\perp/z$ times are equal (the so-called critical balance), where $l_\parallel$ and $l_\perp$ are the typical length scales respectively parallel and perpendicular to the mean magnetic field. Repeating the Kolmogorov arguments, one ends up with an $E(k_\parallel, k_\perp) \sim k_\perp^{-5/3}$ energy spectrum with $k_\parallel \sim k_\perp^{2/3}$. Recently, this result has been generalized in an attempt to model MHD turbulence in both the weak and the strong limits, the ratio of the two time scales τ_A/τ_{NL} being kept fixed but not necessarily of order 1 [15]. In another approach to obtain the transition from the strong to the weak turbulence limit [16,17], the suggested time scale for the energy cascade is given by the inverse average between the Alfvén and the nonlinear time scale $\tau^{-1} = \tau_A^{-1} + \tau_{NL}^{-1}$. All these models, however, assume locality of interactions that are also in question in anisotropic MHD turbulence [18]. A nonlocal model for anisotropic turbulence has been recently proposed by Alexakis [19]; it assumes that the energy cascade is due to interactions between eddies with different parallel sizes and similar perpendicular scales, while a nonuniversal behavior is expected for moderate Reynolds numbers.

Although very useful in getting a first-order understanding of the processes involved in a turbulent cascade, cascade-energy models have to be unavoidably based on assumptions that need to be tested. In this respect, numerical simulations of the MHD equations are very valuable because they provide information about the evolution of the fields in the whole space, something not easily obtained from observations. Many numerical investigations have been performed during the last two decades [20–28] and, at the achieved Reynolds numbers, they have demonstrated that different power-law exponents are obtained depending on the chosen forcing. In this work, we use the results of numerical simulations of freely decaying MHD flows at moderate Reynolds number to investigate the MHD interactions for various intensities of the external magnetic field. In particular, we try to investigate whether the transfer of energy in the parallel and perpendicular direction is local (i.e., the two energies $E^\pm$ cascade between nearby wave numbers) or nonlocal (i.e., distant wave numbers are involved in the cascade), and whether the coupling between the two oppositely moving waves **z**$^+$ and **z**$^-$ (which do not exchange energy) is local or not; and if not, which modes are responsible for the energy cascade.

The paper is organized as follows. In the next section, we give the precise definitions of the transfer functions and partial fluxes used to analyze the nature of the energy cascade. The details of the numerical simulations are given in Sec. III A. In Sec. III B, we investigate the locality or nonlocality of the energy transfers, and in Sec. III C, we examine the nature of the interactions between the two **z**$^+$ and **z**$^-$ fields. We conclude and discuss our results in Sec. IV.

II. DEFINITIONS

Our goal is to investigate the interactions among different scales. To define the notion of "scale," we use the field Fourier transforms

$$\hat{\mathbf{z}}^{\pm}(\mathbf{k}) = \frac{1}{(2\pi)^3} \int \mathbf{z}^{\pm}(\mathbf{x}) e^{-i\mathbf{k}\cdot\mathbf{x}} dx^3 \qquad (3)$$

defined in a 2π-periodic cube, such as

$$\mathbf{z}^{\pm}(\mathbf{x}) = \sum_{\mathbf{k}} \hat{\mathbf{z}}^{\pm}(\mathbf{k}) e^{i\mathbf{k}\cdot\mathbf{x}}. \qquad (4)$$

Similar-size eddies will be considered as the ones whose Fourier transform contains similar wave numbers.

In any basic flow interaction, three wave vectors are involved. For example, the evolution of a given Fourier amplitude $\hat{\mathbf{z}}^{+}(\mathbf{k})$ will be coupled to a $\hat{\mathbf{z}}^{-}(\mathbf{p})$ one and cascade the energy to the mode $\hat{\mathbf{z}}^{+}(\mathbf{q})$ such that the wave vectors satisfy $\mathbf{k}+\mathbf{p}+\mathbf{q}=0$. Note that the mode $\hat{\mathbf{z}}^{-}(\mathbf{p})$ does not gain or lose energy from this interaction since the two energies E^{+} and E^{-} are separately conserved. To obtain the cascade mean rate, one needs to average over all possible triadic interactions. To get a phenomenological understanding of the processes at play in MHD turbulence, we need to know if (i) most of the energetic exchanges occur between wave numbers such that $|\mathbf{k}| \sim |\mathbf{q}|$ and (ii) the energy flux is a result of spectral interactions of the two fields $\mathbf{z}^{\pm}$ with similar wave numbers or not ($|\mathbf{k}| \sim |\mathbf{p}|$).

To address these questions, let us consider a partition of the wave vectors into nonoverlapping sets $S_K^{\pm}$ such that $S^{\pm} = \cup_{K=1}^{\infty} S_K^{\pm} = \mathbb{Z}^3$. For example $S_K^{\pm}$ could be the spherical shells of unit width and radius K, i.e., the set of wave vectors $\mathbf{k}$ that have $K < |\mathbf{k}| \leq K+1$. We now define the filtered fields $\mathbf{z}_K^{\pm}(\mathbf{x})$ so that only modes in the set $S_K^{\pm}$ are kept:

$$\mathbf{z}_K^{\pm}(\mathbf{x}) = \sum_{\mathbf{k} \in S_K^{\pm}} \hat{\mathbf{z}}^{\pm}(\mathbf{k}) e^{i\mathbf{k}\cdot\mathbf{x}}. \qquad (5)$$

Clearly, one gets

$$\mathbf{z}^{\pm}(\mathbf{x}) = \sum_{K} \mathbf{z}_K^{\pm}(\mathbf{x}). \qquad (6)$$

The triadic interactions among the different sets, say $S_K^{\pm}$, $S_P^{\mp}$, and $S_Q^{\pm}$, are given by

$$\mathcal{T}_3^{\pm}(K,P,Q) = -\int \mathbf{z}_K^{\pm} \mathbf{z}_P^{\mp} \cdot \nabla \mathbf{z}_Q^{\pm} dx^3, \qquad (7)$$

which express the rates at which $E^{\pm}$ energies are transferred from the $S_Q^{\pm}$ to $S_K^{\pm}$ sets due to the interactions with the modes belonging to the $S_P^{\mp}$ set. Note that the collection of sets S^{+} and S^{-} need not necessarily be the same; for example, S^{+} could be a collection of cylindrical shells while S^{-} could be a collection of plane sheets. Adding over the index P (all sets in $S^{\mp}$), we obtain the transfer functions

$$\mathcal{T}^{\pm}(K,Q) = \sum_{P} \mathcal{T}_3^{\pm}(K,P,Q) = -\int \mathbf{z}_K^{\pm} \mathbf{z}^{\mp} \cdot \nabla \mathbf{z}_Q^{\pm} dx^3, \qquad (8)$$

which give the E^{+} and E^{-} transfer rates from the $S_Q^{\pm}$ to $S_K^{\pm}$ sets due to all possible interactions. We note here again that the $\mathbf{z}^{+}$ field is not exchanging energy with the $\mathbf{z}^{-}$ field, and vice versa, but their interaction is responsible for the redistribution of the energy among various sets. $\mathcal{T}^{\pm}(K,Q)$ can give us information about the locality or nonlocality of the energy

transfer, i.e., whether the energy is exchanged by nearby sets or long-range transfers from the large scales directly to the small scales are also involved.

However, the $\mathcal{T}^{\pm}(K,Q)$ transfer functions do not give us direct information on the scales of the two fields $\mathbf{z}^{+}$ and $\mathbf{z}^{-}$ that interact and contribute to the energy cascade. To investigate the locality or nonlocality of the interactions between the two Elsässer counterpropagating waves, we introduce the partial fluxes (see [29,30]) defined as

$$\Pi_P^{\pm}(K) = \sum_{K'=0}^{K} \sum_{Q=0}^{\infty} \mathcal{T}_3^{\pm}(K',P,Q) = -\sum_{K'=0}^{K} \int \mathbf{z}_{K'}^{\pm} \mathbf{z}_P^{\mp} \cdot \nabla \mathbf{z}^{\pm} dx^3, \qquad (9)$$

which express the flux of energy out of the outer surface of the $S_K^{\pm}$ shell due to the interactions with the $S_P^{\mp}$ shell. Summation over the whole $S^{\mp}$ collection of sets enables us to recover the usual definition for the global fluxes:

$$\Pi^{\pm}(K) = \sum_{K'=0}^{K} \sum_{Q=0}^{\infty} \sum_{P=0}^{\infty} \mathcal{T}_3^{\pm}(K',P,Q) = -\sum_{K'=0}^{K} \int \mathbf{z}_{K'}^{\pm} \mathbf{z}^{\mp} \cdot \nabla \mathbf{z}^{\pm} dx^3. \qquad (10)$$

In the current work, we are going to use three different types of wave vector collections. We first consider spherical shells traditionally used in studies of isotropic turbulence so that a set S_K contains the wave vectors $\mathbf{k}$ such that $K \leq |\mathbf{k}| < K+1$. The second collection of sets are cylindrical shells along the direction of the guiding magnetic field. In this case, the set S_K contains the wave vectors $\mathbf{k}$ such that $K \leq k_{\perp} < K+1$. Finally, we consider planes perpendicular to the $\mathbf{B}$ direction, so that the set S_K contains the wave vectors $\mathbf{k}$ whose $k_{\parallel}$ component satisfies $K \leq |k_{\parallel}| < K+1$.

III. NUMERICAL RESULTS

A. Numerical setup and initial conditions

We integrate numerically the three-dimensional incompressible MHD equations (1), in a 2π-periodic box using a pseudospectral method with 256^3 collocation points. The time marching uses an Adams-Bashforth Crank-Nicholson scheme, i.e., a second-order finite-difference scheme. The initial kinetic and magnetic fields correspond to spectra proportional to $k^2 \exp(-k/2)^2$ for $k=[1,8]$, which means a flat modal spectrum for wave vector $\mathbf{k}$ up to $k=2$, to prevent any favored wave vector at time $t=0$, and the associated kinetic and magnetic energies are chosen equal, namely, $E_v(t=0) = E_b(t=0) = 1/2$, as in previous numerical studies (see [31] and references therein). Moreover, the correlation between the velocity and magnetic field fluctuations, as measured by the cross-correlation coefficient defined by $2\int \mathbf{v}(\mathbf{x}) \cdot \mathbf{b}(\mathbf{x}) dx^3/(E_v+E_b)$, is initially less than 1%. At scale injection, the initial kinetic and magnetic Reynolds numbers are about 800 for flows at $\nu = \eta \sim 4\times 10^{-3}$, with $u_{\mathrm{rms}} = b_{\mathrm{rms}} = 1$ and an isotropic integral scale $L = 2\pi \int k^{-1} E_v(k) dk / \int E_v(k) dk$ of about π. The dynamics of the flow is then allowed to freely evolve. The parametric study according to the intensity of the background magnetic field $\mathbf{B}$
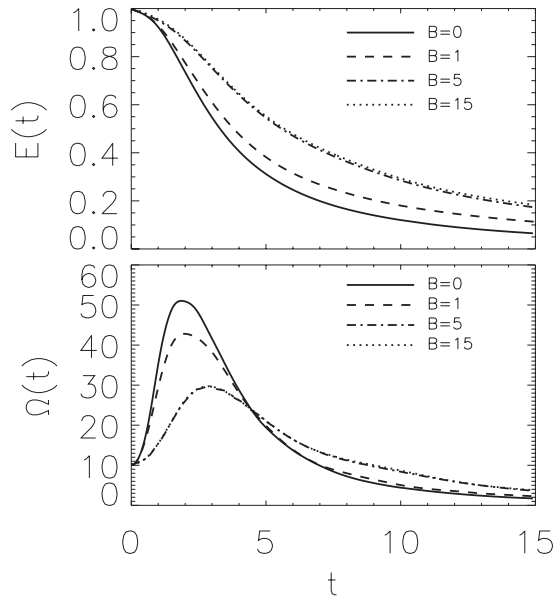
FIG. 1. Temporal evolutions of the total energy (top panel) and of the total enstrophy (bottom panel) for the four examined intensities of the **B** applied field.

is performed for four different values: $B=0$, 1, 5, and 15. All the simulations are run up to a computational time $t_{max}=15$, at which the loss of the total energy (kinetic plus magnetic) is about 95% for the simulation with $B=0$, 90% for $B=1$, and 83% for the $B=5$ and 15 runs.

Figure 1 shows the time evolution of the total energy $E(t)=[E^+(t)+E^-(t)]/2$ and the total enstrophy $\Omega(t)=(1/2)\int[\mathbf{w}^2(\mathbf{x},t)+\mathbf{j}^2(\mathbf{x},t)]dx^3$ (where $\mathbf{w}=\nabla\times\mathbf{u}$ stands for the vorticity field, and $\mathbf{j}=\nabla\times\mathbf{b}$ for the current), for the four different simulations. One can note that the influence of the strength of the external magnetic field clearly slows down the flow dynamics. Note that the $B=5$ and 15 flows present a very similar temporal behavior in energy as well as in enstrophy. The analysis that follows in the next section is based on the outputs of the runs at $t=4$ where the spectra are fully developed and all runs have roughly the same enstrophy. At this time, the cross-correlation coefficient, which one can also write $(E^+-E^-)/(E^++E^-)$, is about 3.6% and 2.5%, respectively, for the $B=0$ and 1 flows, while it is close to 1.6% for $B=5$ and 1% for $B=15$, with thus a lesser increase in the more strongly magnetized flows. The energy spectra in the perpendicular direction to the uniform **B** field $E(k_\perp)=(1/2)\int[\hat{\mathbf{z}}^-(k)]^2+[\hat{\mathbf{z}}^+(k)]^2 k_\perp dk_\parallel$ and in the parallel one $E(k_\parallel)=(1/2)\int[\hat{\mathbf{z}}^-(k)]^2+[\hat{\mathbf{z}}^+(k)]^2 k_\perp dk_\perp$ are shown in Fig. 2 at the same time. Clearly as the magnetic field intensity is increased, the spectrum in the $k_\parallel$ direction becomes steeper. Because the planes at $k_\parallel=0$ and $k_\parallel=1$ are shown to play an important role in the cascade, we mention here their properties in more detail. In absence of the applied magnetic field, the modes with $k_\parallel=0$ contain 32% of the total energy and 8% of the total enstrophy, and the $k_\parallel=1$ modes have 30% of the total energy and 10% of the total enstrophy. In the strongly anisotropic case, $B=15$, the $k_\parallel=0$ modes contain 55% of the total energy and 34% of the total enstrophy while the $k_\parallel=1$ modes have 37% of the total energy and 35% of the total enstrophy.
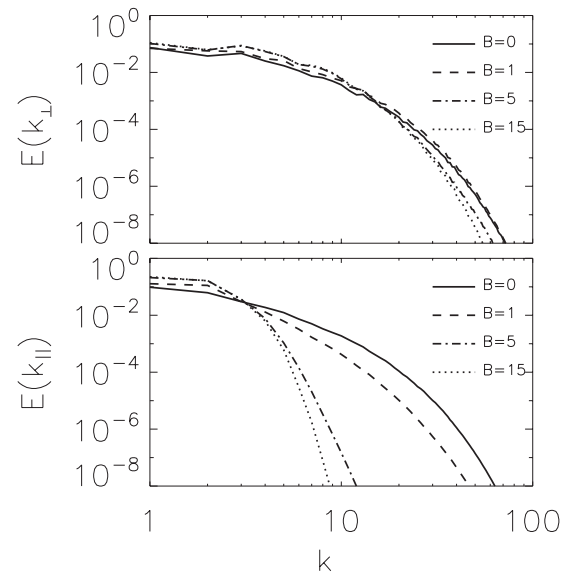
FIG. 2. Total energy spectra in the perpendicular (top panel) and parallel (bottom) directions.

In our investigation, we focus on the cascade of the E^- energy. The E^+ cascade has also been analyzed and it gives qualitatively similar results. We consider separately the cascades in the perpendicular and parallel directions relative to the applied magnetic field. For this reason, we examine three different types of flux: (i) the flux across spheres of radius $k\equiv|\mathbf{k}|$ which corresponds to an isotropic analysis, (ii) the flux across cylinders of radius $k\equiv k_\perp$ which corresponds to the flux in the perpendicular direction, and (iii) the flux across planes located at $k\equiv|k_\parallel|$, which corresponds to the flux in the direction parallel to the **B** field direction. Figure 3 shows these three fluxes, as a function of k, for various **B**
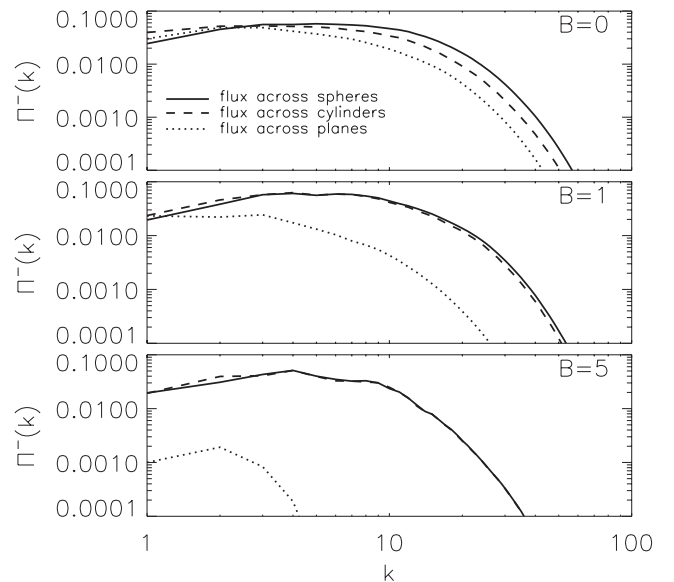
FIG. 3. Fluxes $\Pi^-(k)$ across (i) spheres (solid line), (ii) cylinders (dashed line), (iii) planes (dotted line), for $B=0$ (top panel), 1 (middle panel), and 5 (bottom panel).
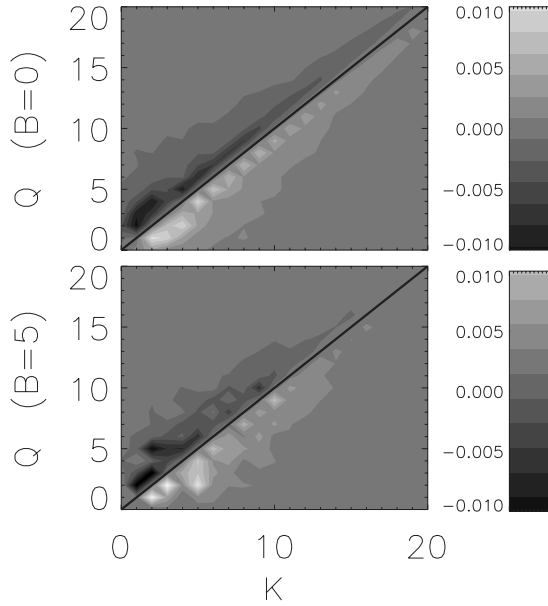
FIG. 4. Transfer function $\mathcal{T}^-(K,Q)$ which demonstrates the energy exchange between cylindrical shells of radii K and Q. Solid lines show the diagonal $K=Q$. The top panel shows the $B=0$ case and the bottom panel the $B=5$ case.

intensities. It is clear that, as the amplitude of the large-scale magnetic field is increased, the parallel flux is strongly reduced. For $B=5$, this flux is reduced by more than one order of magnitude when compared to the case with $B=0$. For $B=15$, the parallel flux across planes is very small and it even takes negative values.

B. Energy transfers

We now examine the locality or nonlocality of energy transfers from our numerical data. For two different values of the uniform magnetic field, namely $B=0$ and 5, Fig. 4 shows a shadow graph of the transfer function $\mathcal{T}^-(K,Q)$ between $\mathbf{z}_K^-$ and $\mathbf{z}_Q^-$, defined in Eqs. (5) and (8), for energy exchanges across cylindrical shells (perpendicular cascade), while Fig. 5 shows the transfer function $\mathcal{T}^-(K,Q)$ for energy exchanges across plane sheets (parallel cascade). In all cases, the transfer is concentrated along the diagonal $K=Q$ line. This indicates that the cascade happens through a local energy exchange. Similar results are obtained from the two other simulations at $B=1$ and 15 (not shown). Note the highly nonlinear color bar used for the parallel cascade in the $B=5$ case. This choice is due to the extremely fast decrease of the amplitude of $\mathcal{T}^-(K,Q)$ as the wave numbers K and Q become large. From Figs. 4 and 5, it can be seen that most of the energy exchange happens close to the diagonal line ($K=Q$). In a strong B flow, some inverse cascade is also visible in the parallel cascade (Fig. 5) as indicated by the dark lines below the diagonal and the bright ones above the diagonal.

To get a better understanding of the $\mathcal{T}^\pm(K,Q)$ transfer functions, we look at a single wave number Q. Figure 6 displays $\mathcal{T}^-(K,Q)$ for the perpendicular cascade (cylinders)

at $Q=10$ as a function of K, whereas Fig. 7 shows it for the parallel cascade (planes) at $Q=10$. To compare the results obtained from the different B cases, the $\mathcal{T}^-(K,Q)$ amplitudes are normalized so that all transfers are of the same order of magnitude. Positive values of $\mathcal{T}^-(K,Q)$ imply that the shell K receives energy from the shell $Q=10$ (Fig. 6, perpendicular case) and (Fig. 7, parallel case) while negative values of $\mathcal{T}^-(K,Q)$ mean that the shell K gives energy to the shell $Q=10$.

For the perpendicular cascade, the shell $Q=10$ receives most energy from slightly smaller wave numbers than $K=10$ and it gives energy to slightly larger wave numbers. This implies a locality in the energy transfer, since it is mostly the nearby cylindrical shells that exchange energy. The parallel cascade presents a similar behavior; the shell $Q=10$ receives energy from slightly smaller wave numbers than $K=10$ and it gives energy to slightly larger wave num-

FIG. 5. Transfer function $\mathcal{T}^-(K,Q)$ which demonstrates energy exchanges between plane sheets located at distance K and Q from origin, for $B=0$ (top panel) and 5 (bottom panel) cases. Solid lines indicate the $K=Q$ diagonal.
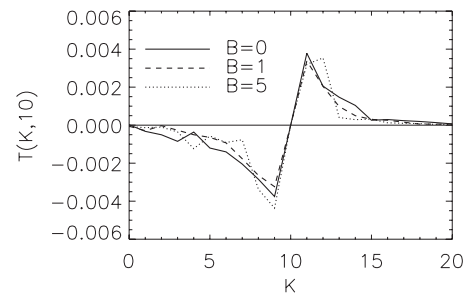
FIG. 6. Energy transfer function $\mathcal{T}^-(K,Q)$ for the perpendicular cascade (cylinders) for $Q=10$ as a function of K, from the runs with $B=0$ (solid line), 1 (dashed line), and 5 (dotted line). Amplitudes of $\mathcal{T}^-(K,Q)$ are normalized to have the same order of magnitude as in the $B=0$ case.
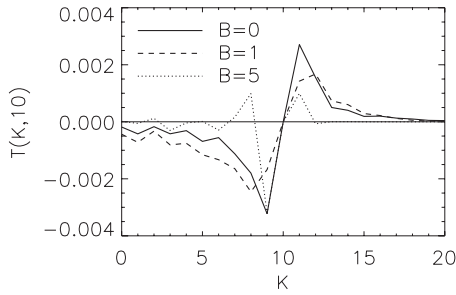
FIG. 7. Energy transfer function $\mathcal{T}^-(K,Q)$ for the parallel cascade (planes) for $Q=10$ as a function of K, from the data at $B=0$ (solid line), 1 (dashed line), and 5 (dotted line). Amplitudes of $\mathcal{T}^-(K,Q)$ are normalized to have the same order of magnitude as in the $B=0$ case.

bers. Note, however, that for the $B=5$ flow, there is also some trace of an inverse cascade (energy transfer from the wave number $Q=10$ to the wave number $K=8$). This local behavior has also been found in isotropic ($B=0$) decaying MHD turbulence simulations [32]. Nevertheless, we need to note that in forced MHD turbulence where the magnetic field is generated by dynamo action, strong nonlocal transfers also exist [6,8]. Whether these nonlocal transfers are present in the forced anisotropic regime still needs further studies.

C. Nonlinear interactions between z^+ and z^-

The analysis of the energy transfer functions has thus shown that the energy cascades locally, which means that, in a collision of two waves, the waves are distorted into structures of only slightly smaller scales. Nonetheless, this does not mean that interactions among oppositely traveling waves are local. In the limit of very large intensities of the background magnetic field, where the weak turbulence theory is valid, the energy cascade is due to interactions with the modes in the plane at $k_\parallel=0$. Therefore, modes with $k_\parallel \geqslant 1$ interact with modes $k_\parallel \ll 1$ to cascade the energy. To that respect, the interactions are nonlocal since short waves (large $k_\parallel$) interact with long waves (small $k_\parallel$) to cascade the energy. To investigate how close to the weak turbulence regime we are, we plot in Fig. 8 the total energy flux $\Pi^-(K)$, defined in Eq. (10), across cylinders, together with the partial flux $\Pi^-_{P=0}(K)$, defined in Eq. (9), due to interactions with just $k_\parallel=0$ modes. As the strength of the uniform magnetic field is increased, the flux due to the interactions with the $k_\parallel=0$ modes become more and more dominant. In the $B=15$ flow, the global and partial fluxes across cylinders become almost indistinguishable, suggesting that interactions with the modes in the plane at $k_\parallel=0$ are responsible for the energy cascade. This means that the flow dynamics tends to be closer to a weak turbulence regime where the three-wave resonant interactions are dominating.

A different behavior is obtained for the parallel energy cascade. When a mode $\hat{\mathbf{z}}^-(\mathbf{k})$ interacts with a mode $\hat{\mathbf{z}}^+(\mathbf{p})$, the $\hat{\mathbf{z}}^-(\mathbf{k})$ energy will move to the wave vector $\mathbf{q}$ so that the relation $\mathbf{k}+\mathbf{p}+\mathbf{q}=\mathbf{0}$ holds. If, however, $\mathbf{p}$ belongs to the wave vector set with $p_\parallel=0$, this relation then reads
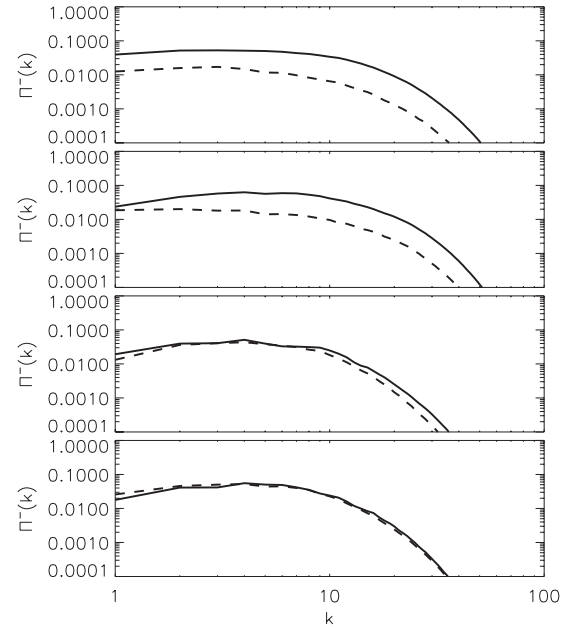
FIG. 8. Total energy flux $\Pi^-(K)$ (solid line) across cylinders of radius K together with the partial flux $\Pi^-_{P=0}(K)$ (dashed line) for the four different values of B, from $B=0$ (top panel) up to $B=15$ (bottom panel).

$k_\parallel+q_\parallel=0$ in the parallel direction, i.e., $|k_\parallel|=|q_\parallel|$. Therefore, the energy remains in spectral planes located at the same distance from the origin. As a result, interactions with the $k_\parallel=0$ modes cannot contribute to the energy cascade in the parallel direction. In this case, the closest modes to the $k_\parallel=0$ modes are the ones that gives most of the energy flux. Figure 9 shows the total energy flux across planes and the partial flux due only to interactions with the modes in the plane at $k_\parallel=1$ (the closest to the $k_\parallel=0$ plane). As the amplitude of the **B** field is increased, most of the parallel flux comes from modes with $k_\parallel=1$. Here, we need to note that the flux in the parallel direction is much noisier than the flux in the perpendicular direction and that it often presents negative values (absolute values are plotted in the bottom panel of Fig. 9). A thorough analysis of the parallel cascade would require to average many data outputs which is not possible in the case of a freely decaying flows. Such an analysis is left for future work.

IV. CONCLUSION AND DISCUSSION

In this work we examine the energy cascade and the interactions between different scales for freely decaying MHD flows in the presence of a uniform magnetic field. Our analysis is based on data obtained from direct numerical simulations of the MHD equations with four different intensities of the applied magnetic field, in an attempt to study the transition from strong to weak turbulence limit. One clearly established result is that, as the strength of the uniform magnetic field is increased, the energy spectrum becomes anisotropic with most of the energy concentrated in the small $k_\parallel$ wave numbers, as already known [28]. It is further shown that the
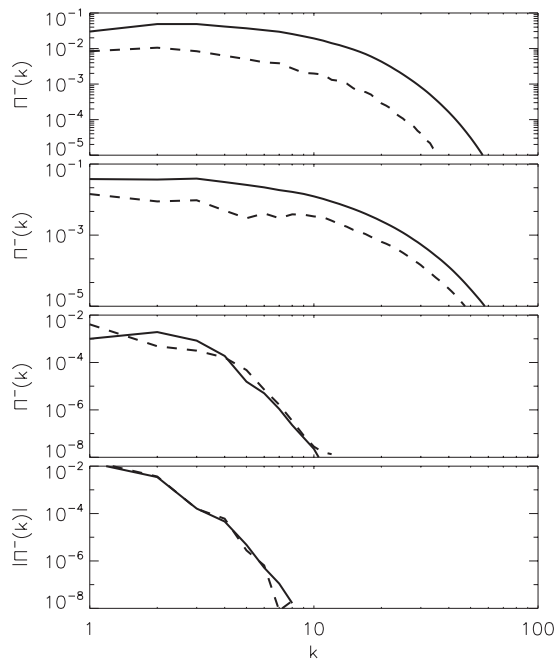
FIG. 9. Total energy flux $\Pi^-(K)$ (solid line) across planes at $k_\parallel$ $=K$ together with the partial flux $\Pi^-_{P=1}(K)$ (dashed line) for the four different values of B from $B=0$ (top panel) up to $B=15$ (bottom panel). Note the absolute value in the latter case.

energy flux in the parallel direction (relative to the uniform magnetic field) is also strongly suppressed when the guiding field is introduced.

To investigate the locality or nonlocality of the spectral interactions, we measure the transfer functions for the parallel and perpendicular cascades. The transfer functions in the parallel and perpendicular directions are found to be local, whatever the strength of the external magnetic field. As a result, the coupling between modes that travel in the same direction is local and the energy exchange occurs between similar-size eddies. This behavior has been shown to hold in decaying isotropic MHD turbulence simulations (with $B=0$) [32]. However, in the presence of a mechanical forcing, strong nonlocal interactions have been observed with a direct energy transfer from the forced scale to the inertial range scales [6,8]. Whether this nonlocal behavior persists in the anisotropic case still needs further investigation.

The locality or nonlocality of the interactions between oppositely moving waves (z^+ and z^-), which do not exchange energy, is measured by means of partial fluxes in the parallel and perpendicular directions due to the coupling in different spectral planes. This coupling between oppositely propagating modes does not appear local. As the amplitude of the applied magnetic field is increased, most of the interactions occur with the $k_\parallel=0$ modes that are dominant in cascading the energy. Most of the energy flux is thus in the perpendicular direction, since the $k_\parallel=0$ modes do not contribute to the energy cascade in the parallel direction. Hence, the more strongly magnetized flows tend to present a dynamics close to the weak turbulence limit, where the three-wave resonant interactions are responsible for the cascade process. This also partly explains the similar temporal evolution in the $B=5$ and 15 regimes (see Fig. 1) since, in both cases, most of the cascade is due to the $k_\parallel=0$ modes.

For the parallel cascade, the interactions are slightly different. As already said, this is due to the inability of the $k_\parallel=0$ modes to cascade the energy in the parallel direction. In that case, the modes with the smallest but nonzero $k_\parallel$ ($k_\parallel \simeq 1$) are the ones responsible for the cascade. This behavior is in qualitative agreement with the description of a recent phenomenological model [19]. However, the lack of resolution does not allow us to pursue a quantitative comparison.

Finally, we would like to emphasize that we analyze here numerical data of freely decaying MHD flows submitted to an external magnetic field whose amplitude is varied, while all the other parameters are kept unchanged (periodic boundary conditions, unit magnetic Prandtl number, initial conditions, and Reynolds number). Thus, one should be cautious in any attempt to generalize the obtained results, e.g., forced turbulence could lead to different behaviors and should be studied separately. The results could also be dependent on the kinetic Reynolds number as well as on the magnetic Prandtl number. Furthermore, the use of a refined spectral grid in the parallel direction, allowing the presence of more modes with $k_\parallel \ll 1$, could alter the energy cascade.

[1] Ya. B. Zeldovich, A. A. Ruzmaikin, and D. D. Sokoloff, *Magnetic Fields in Astrophysics* (Gordon & Breach Science Publications, New York, 1990).

[2] A. N. Kolmogorov, Dokl. Akad. Nauk SSSR **30**, 299 (1941).

[3] T. A. Yousef, F. Rincon, and A. A. Schekochihin, J. Fluid Mech. **575**, 111 (2007).

[4] M. K. Verma, Phys. Rep. **401**, 229 (2004).

[5] M. K. Verma, A. Ayyer, and A. V. Chandra, Phys. Plasmas **12**, 82307 (2005).

[6] A. Alexakis, P. D. Mininni, and A. Pouquet, Phys. Rev. E **72**, 046301 (2005).

[7] P. Mininni, A. Alexakis, and A. Pouquet, Phys. Rev. E **72**, 046302 (2005).

[8] D. Carati, O. Debliquy, B. Knaepen, B. Teaca, and M. K. Verma, J. Turbul. **7**, 1 (2006).

[9] S. Galtier, S. V. Nazarenko, A. C. Newell, and A. Pouquet, Astrophys. J. **564**, L49 (2002).

[10] S. Galtier, S. V. Nazarenko, A. C. Newell, and A. Pouquet, J.

Plasma Phys. **63**, 447 (2000).

[11] S. V. Nazarenko, A. C. Newell, and S. Galtier, Physica D **152-153**, 646 (2001).

[12] P. Iroshnikov, Sov. Astron. **7**, 566 (1963).

[13] R. Kraichnan, Phys. Fluids **8**, 1385 (1965).

[14] P. Goldreich and S. Sridhar, Astrophys. J. **438**, 763 (1995).

[15] S. Galtier, A. Pouquet, and A. Mangeney, Phys. Plasmas **12**, 092310 (2005).

[16] W. H. Matthaeus and Y. Zhou, Phys. Fluids B **1**, 1929 (1989).

[17] Y. Zhou, W. H. Matthaeus, and P. Dmitruk, Rev. Mod. Phys. **76**, 1015 (2004).

[18] A. Bhattacharjee and C. S. Ng, Astrophys. J. **548**, 318 (2001).

[19] A. Alexakis, Astrophys. J. **667**, L93 (2007).

[20] D. Biskamp and W. C. Müller, Phys. Plasmas **7**, 4889 (2000).

[21] J. Cho and E. T. Vishniac, Astrophys. J. **539**, 273 (2000).

[22] P. Dmitruk, D. O. Gomez, and W. H. Matthaeus, Phys. Plasmas **10**, 3584 (2003).

[23] J. Mason, F. Cattaneo, and S. Boldyrev, e-print arXiv:0706.2003v1.

[24] J. Maron and P. Goldreich, Astrophys. J. **554**, 1175 (2001).

[25] W. C. Müller and R. Grappin, Phys. Rev. Lett. **95**, 114502 (2005).

[26] C. S. Ng and A. Bhattacharjee, Astrophys. J. **465**, 845 (1996).

[27] C. S. Ng, A. Bhattacharjee, K. Germaschewski, and S. Galtier, Phys. Plasmas **10**, 1954 (2003).

[28] S. Oughton, E. R. Priest, and W. H. Mattaheus, J. Fluid Mech. **280**, 95 (1994).

[29] A. Alexakis, P. D. Mininni, and A. Pouquet, Phys. Rev. Lett. **95**, 264503 (2005).

[30] P. D. Mininni, A. Alexakis, and A. Pouquet, Phys. Rev. E **74**, 016303 (2006).

[31] L. J. Milano, W. H. Matthaeus, P. Dmitruk, and D. C. Montgomery, Phys. Plasmas **8**, 2673 (2001).

[32] O. Debliquy, M. K. Verma, and D. Carati, Phys. Plasmas **12**, 042309 (2005).